



# Propagation of friction parameter uncertainties in the nonlinear dynamic response of turbine blades with underplatform dampers



Jie Yuan<sup>a,b,\*</sup>, Alfredo Fantetti<sup>a</sup>, Enora Denimal<sup>a</sup>, Shubham Bhatnagar<sup>a</sup>, Luca Pesaresi<sup>a</sup>, Christoph Schwingshackl<sup>a</sup>, Loic Salles<sup>a</sup>

<sup>a</sup>Vibration University Technology Centre, Imperial College London, SW72AZ London, UK

<sup>b</sup>Aerospace Centre of Excellence, University of Strathclyde, G11XQ Glasgow, UK

## ARTICLE INFO

### Article history:

Received 2 August 2020

Received in revised form 11 January 2021

Accepted 19 January 2021

Available online 16 February 2021

### Keywords:

Underplatform dampers

Uncertainty quantification

Nonlinear dynamics

Friction and contact

Sobol indices

Polynomial chaos expansion

## ABSTRACT

Underplatform dampers are widely used in turbomachinery to mitigate structural vibrations by means of friction dissipation at the interfaces. The modelling of such friction dissipation is challenging because of the high variability observed in experimental measurements of contact parameters. Although this variability is not commonly accounted for in state-of-the-art numerical solvers, probabilistic approaches can be implemented to include it in dynamics simulations in order to significantly improve the estimation of the damper performance. The aim of this work is to obtain uncertainty bands in the dynamic response of turbine blades equipped with dampers by including the variability observed in interfacial contact parameters. This variability is experimentally quantified from a friction rig and used to generate uncertainty bands by combining a deterministic state-of-the-art numerical solver with stochastic Polynomial Chaos Expansion (PCE) models. The bands thus obtained are validated against experimental data from an underplatform damper test rig. In addition, the PCEs are also employed to perform a variance-based global sensitivity analysis to quantify the influence of contact parameters on the variation in the nonlinear dynamic response via Sobol indices. The analysis highlights that the influence of each contact parameter in vibration amplitude strongly varies over the frequency range, and that Sobol indices can be effectively used to analyse uncertainties associated to structures with friction interfaces providing valuable insights into the physics of such complex nonlinear systems.

© 2021 Elsevier Ltd. All rights reserved.

## 1. Introduction

Aeroengines typically undergo a wide range of operating conditions in flights and as a result it is not possible to avoid all critical resonances in their bladed disks [1–3]. Reducing the vibration levels at these resonant frequencies is the main option to guarantee aeroengine durability and reliability by mitigating the threat of high-cycle fatigue resulting from large resonance stresses. A common method to reduce vibration levels in a bladed disk is the introduction of dry friction damping, which provides high damping at a low cost through rubbing motions on the contact interfaces [4]. Among friction dampers,

\* Corresponding author at: Vibration University Technology Centre, Imperial College London, SW72AZ London, UK.

E-mail addresses: [jie.yuan@imperial.ac.uk](mailto:jie.yuan@imperial.ac.uk), [jie.yuan@strath.ac.uk](mailto:jie.yuan@strath.ac.uk) (J. Yuan).

underplatform dampers (UPDs) are the most common source of damping in turbine disks. UPDs are metallic devices usually placed in the groove under the platforms of two adjacent blades and kept in contact with the platforms by the centrifugal loads during operation. When blades vibrate, the relative displacement between the platforms and the damper creates friction at the contact surfaces that leads to a large energy dissipation with a consequent reduction in the resonance amplitude. Due to the frictional nature of the problem, the dynamic response of a bladed disc equipped with UPDs is strongly nonlinear, with both the vibration levels and resonance frequencies being amplitude dependent.

A number of approaches have been developed in the past few decades to model the dynamics of jointed structures with friction interfaces. The simplest models are those relying on the use of linear mass-spring models, coupled with nonlinear macro-elements that consist of either parallel or series springs, dash pots, and Coulomb friction sliders [5–8]. However, these models generally fail to accurately represent the physics on the contact interface. On the other hand, there are also high-fidelity joint models that are produced by the solid mechanics communities. Two main types of these predictive models are: (1) a whole joint approach based on a time-domain solver [9,10]; (2) a frequency-domain approach based on the multi-harmonic balance method (MHBM) [11]. A detailed comparison of these two approaches can be found in [8]. The frequency-domain approach is employed in this study to obtain accurate estimations of the dynamic response of turbines, starting from previous work of the authors to help the design and optimization of the UPDs [12]. This modelling approach is based on MHBM, hybrid reduction techniques and elastic contact models, and is extremely efficient in capturing the nonlinear behavior for turbines with UPDs. Its reliability largely depends on the accurate characterization of the contact parameters that describe the friction mechanisms occurring at the contact interfaces [13,14], since the UPD performance is very sensitive to the interface geometry. Unfortunately, the contact parameters describing these friction mechanisms involve large uncertainties due to the complexity of the physical phenomena at the contact interfaces [15–18]. For this reason, commonly used deterministic modelling approaches might lead to errors in the predictions.

The friction contact is modelled in turbine applications by means of a few parameters, namely the friction coefficient, the normal and tangential contact stiffness and the normal pressure. These contact parameters are usually obtained experimentally by means of fretting test rigs [19–26] since current contact models are not yet capable of providing accurate predictions of those parameters. In addition, a large variability is often observed in experiments due to the complex phenomena taking place at the contact interfaces, such as fretting wear [16]. Thus, to ensure a good level of accuracy in nonlinear response predictions, the uncertainties in the contact parameters must be quantified experimentally and propagated into the nonlinear response simulations.

To address this issue, many researchers have studied the impact of contact uncertainties in dynamic analysis through different numerical strategies. One of the approaches to include these uncertainties from contact interfaces is to develop more advanced physics-based model. For example, an advanced multi-scale modeling approach was developed [27] to take into account the effects of roughness, fretting wear and waviness. The disadvantage of such an approach is the associated high computational cost. Also, some input parameters for the multi-scale model that include roughness and contact stiffness dependence are difficult to obtain experimentally. Another approach to include uncertainties from contact interfaces is to treat these micro-scale effects as an uncertainty source. Petrov [14] employed a sensitivity approach to study the impact of uncertainty of the friction coefficient and of geometric parameters of the UPD on the nonlinear dynamic behaviour of bladed disks. The Probability Density Functions (PDF) of the forced response for given frequencies were reconstructed from the sensitivities, demonstrating the high influence of the friction coefficient on the dynamics of the structure. Krack et al. [13] performed a reliability analysis of a cyclic blisk with nonlinear shroud coupling subjected to the uncertainties in contact interfaces, showing again a large impact of the contact parameters. Butlin et al. [28,29] developed an approach based on the Maximum Entropy to estimate the response distribution for a structure with friction, which was validated against experimental data by a test rig that represents friction damper assemblies. Delaune et al. [30] numerically investigated the impact of uncertainties on fretting wear and showed that a large variety of vibration behaviours can be observed when uncertainty is considered. Recently, Gastaldi et al. [17] experimentally investigated the effect of surface finish on the function of underplatform dampers, showing a large impact of the contact interface conditions on the dynamic response. Comparisons between measured data and predictions from nonlinear models also showed the uncertainty in the dynamic performance of underplatform dampers due to the contact interface [31–33]. These different works demonstrate the high influence of friction contact uncertainties from the contact interface on the dynamic response of structures with friction, and highlight the necessity to take them into consideration. However, the uncertainties from the input contact parameters have not been experimentally quantified in the aforementioned work, nor have they been propagated in the nonlinear vibration response.

A classic method to propagate the uncertainty is the use of Monte Carlo Simulations (MCS) through repeated deterministic experiments [34,30]. The popularity of the MCS is due to their high computational robustness with respect to the dimension and the performance function of the problem. The main drawback of the standard MCS is that it requires a large number of samples to ensure the representation of the entire parameter range and hence leads to heavy computational costs for high dimension problems [35], such as a large nonlinear dynamic system with UPDs. As a consequence, some specific strategies are needed to accelerate the convergence of MCS by using specific sampling techniques such as Latin Hypercube Sampling (LHS) [36]. Another strategy consists of using surrogate modelling methods to represent the expensive simulations of the model. From a relatively small number of evaluations of the expensive model, a mathematical function that approximates it is constructed. This function has a computational cost that is almost null and therefore can be used to perform a large number of MCS to propagate the uncertainty or to perform any sensitivity analysis. Different surrogate modelling approaches exist, as Kriging [37], Support Vector Machine (SVM)[38] or the Generalized Polynomial Chaos Expansion

(PCE) [39,40]. The latter is based on a stochastic description of the uncertain parameters and comprises the projection of the random variable on a polynomial basis orthogonal with respect to the PDF. This approach has already proven its efficiency for the uncertainty propagation of linear and nonlinear FRFs [41–43]. The PCE has also been coupled with multi-harmonic balance methods to investigate the effects of the uncertainties in nonlinear systems [44,45]. One of the main advantages of the PCE is that it can be exploited without any additional simulation to directly determine the mean and the variance of the process, but also to perform a variance-based sensitivity analysis based: Sobol analysis [46,47] and for this reason has been used in the present study.

The objective of the present study is to quantify the impact of contact uncertainties from friction interfaces on the dynamics of turbine blades with UPDs and to obtain uncertainty bands on the nonlinear forced responses. The main novelty is that the distribution of uncertain contact parameters from friction interfaces is experimentally quantified and propagated in the nonlinear vibration response with a state-of-the-art surrogate modeling technique. Furthermore, the effects of each uncertain parameter on the variability of the nonlinear vibration response are then studied using a variance based sensitivity analysis. This demonstrates the interest of using such tools to have insights into the influence of each contact parameter in a wide range of excitation levels. The paper is organized as follows: the numerical strategy employed for the computation of the nonlinear dynamic behaviour of the system is firstly presented as well as the underlying mechanical model; secondly, the uncertainties related to the contact parameters are experimentally estimated; these uncertainties are then numerically propagated in the model with PCE and compared against experimental data from an UPD test rig. Finally, the PCE meta models are further exploited by performing a Sobol analysis to study the impact of the contact parameters on the blade dynamics.

## 2. Deterministic simulations

This section describes the deterministic simulations used to predict the dynamic response of turbine structures with UPDs. The MHBM based simulation approach is firstly described and then the reference FE model is presented. This model replicates the UPD test rig from Imperial College London (hereafter referred to as Imperial) [12] used in this study. Finally, the resulting nonlinear frequency responses are discussed.

### 2.1. Nonlinear frequency simulation approach

The nonlinear frequency responses are computed using the solver FORSE (**F**orce **R**esponse **S**uit**E**) that has been developed by the Vibration University Centre at Imperial, and is based on the multi-harmonic balance method (MHBM) coupled with the Alternating Time/Frequency technique (AFT) [48]. Detailed information about the solver can be found in [11], but for completeness a short description will be provided here. The solver aims at finding the solution of the nonlinear dynamic equilibrium equations that describe the system:

$$\mathbf{M}\ddot{\mathbf{x}}(t) + \mathbf{C}\dot{\mathbf{x}}(t) + \mathbf{K}\mathbf{x}(t) + \mathbf{F}_{nl}(\dot{\mathbf{x}}(t), \mathbf{x}(t)) = \mathbf{F}_{ex}(t) \quad (1)$$

where  $\mathbf{M}$ ,  $\mathbf{C}$ ,  $\mathbf{K}$  are the mass, damping and stiffness matrices;  $\mathbf{x}(t)$  is the vector of displacement of all the DOFs and the dots denote the derivative with respect to time.  $\mathbf{F}_{ex}$  is the vector of external excitation forces and  $\mathbf{F}_{nl}$  is the time dependent vector of friction forces occurring at the contact between the damper and blades. The basic idea of the MHBM is to decompose the nonlinear dynamic response using a truncated Fourier series with  $n$  harmonics:

$$\mathbf{x}(t) = \mathbf{Q}_0 + \sum_{j=1}^n \mathbf{Q}_j^c \cos(m_j \omega t) + \mathbf{Q}_j^s \sin(m_j \omega t) \quad (2)$$

where  $\mathbf{Q}_0$  is the 0<sup>th</sup> order harmonic coefficient and  $\mathbf{Q}_j^c$ ,  $\mathbf{Q}_j^s$  are the sinusoidal harmonic coefficients for each DOF. Using the Galerkin projection, a system of algebraic equations in a frequency domain are then obtained that can be solved with a Newton–Raphson method for the harmonic coefficients [11]. In order to track the nonlinear forced response over a range of frequencies, the continuation technique that includes prediction (secant method) and correction (arc length) stages is employed [49], which is able to capture any softening or hardening behaviour. A hybrid reduced order modelling (ROM) technique is also used to significantly reduce the system DOFs, by retaining only the nonlinear DOFs on the contact interface [11]. More details with respect to MHBM, AFT, ROM and continuation techniques can be found in [49,50]. The solutions obtained by the nonlinear solver strongly depend on the friction forces from the contact between damper and platforms. Hence, a reliable contact model is required for such computations.

### 2.2. Contact friction model

The approach to compute the nonlinear friction forces is to model the contact interfaces as dense mesh grids of contact nodes, which are connected by contact elements. A 3D contact element is typically used in nonlinear dynamic simulations of systems with friction, which consists of two coupled Jenkins elements to model a two-dimensional in-plane motion, and a coupled spring in the normal direction as shown in Fig. 1a. The springs in the different directions model the tangential and normal contact stiffnesses. The relation between forces and displacements at the contact depends on the contact state, as described in the following. Normal contact conditions are defined by two states, namely in-contact condition and separation

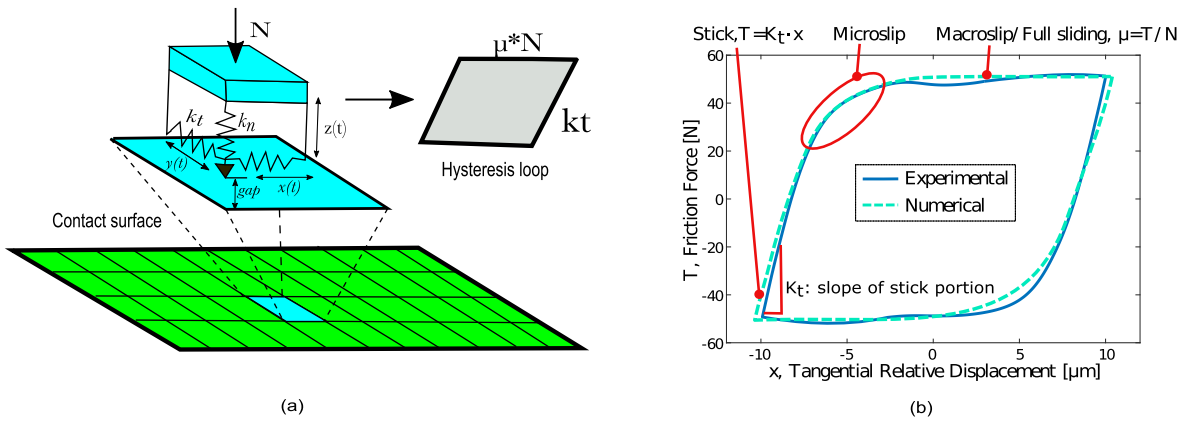


Fig. 1. (a) Meshed interface and 3D node to node contact friction element (b) Experimental identification of contact parameters.

condition. If the predicted normal force  $F_N$  becomes negative, separation occurs between the two contact nodes and the normal contact force becomes zero. Whereas if  $F_N$  is positive, the contact pair is in contact and thus there are two types of tangential contact states: one is the sticking condition (i.e. the tangential contact force  $F_T$  is less than the Coulomb friction limit  $\mu F_N$ ) and the other is the slipping condition (i.e. the tangential contact force  $F_T$  is equal the Coulomb friction limit  $\mu F_N$ ). The interested readers can also find the detailed formulation of this contact element in [51].

The hysteresis loop obtained from a single 3D contact element with constant normal load is shown in Fig. 1a. The hysteresis loop obtained from a full mesh grid of contact elements is shown in Fig. 1b and is compared with a typical experimental loop. Experimental loops include sticking, microslip and macroslip states. Microslip occurs when a part of the interface is in sliding condition while the rest is in sticking, and cannot be captured by a single 3D element, which indeed can only be in full stick or macroslip. However, the combination of lots of contact elements in the dense mesh grid discretization of the contact interface makes it possible to model the typical microslip behavior observed in the experimentally measured loops as shown in Fig. 1b, since some of the elements will be in stick and some will slip. This further confirms that 3D contact elements are effective to represent the contact friction behaviour, and also that the experimental identification of their contact parameters must be accurate.

Obviously, the contact friction for each contact node can be discontinuous and non-smooth once the slipping happens. However, such a non-smooth motion can still be approximated by continuous multi-harmonic functions using MHBM. The accuracy of such an approximation depends on the number of harmonics used. A convergence study is therefore often required to determine the number of harmonics that should be used in the simulation. In terms of implementation of MHBM, the AFT procedure [50] is commonly used for such an approximation. This scheme mainly consists two steps: the non-smooth contact friction force is firstly evaluated following the iDFT procedure to transform the dynamic response from frequency domain to time domain; then, this non-smooth contact force is approximated using multi-harmonic coefficients using the DFT procedure. This procedure has been proved to be very accurate if sufficient harmonics are used [4].

### 2.3. Reference UPD model

Fig. 2a shows the real setup of the UPD test built at Imperial for the validation of the in-house nonlinear solver [11] used to perform simulations for turbine systems with UPDs. Fig. 2b shows the 3D FE model of the UPD rig, which consists of two

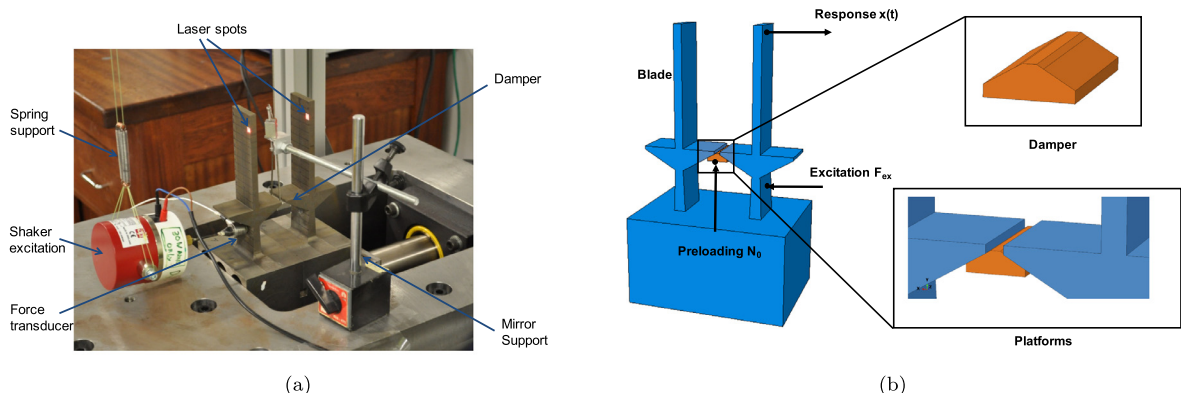


Fig. 2. (a) Under platform damper test rig at Imperial [12]; (b) 3D representation of the UPD rig.

beam-like blades with platforms on each side that are fixed on a common base which simulates a rigid disk, and an UPD in orange that sits between the two blades and is held in contact by a pulley loading system as shown in Fig. 2a. The UPD is modelled as a classical cottage roof damper. The mesh for FE modelling was generated by Hyperwork, which is composed of 54,972 quadratic hexahedral elements. A stainless-steel material is used, i.e. the Young modulus is equal to 197 GPa and the density is equal to 7800 kg/m<sup>3</sup>. For a detailed description of the system, the reader is invited to refer to [12]. The first two modes of the turbine blades correspond to the in-phase and out-of-phase first bending mode of the blades, and their natural frequencies are 269.9 Hz and 269.8 Hz, respectively. The in-phase mode occurs when two blades flap in the same direction while the out-of-phase mode does when they move toward each other. These two modes represent the fundamental movement of the turbine blade platform under investigation and are described in the next section.

#### 2.4. Forced frequency response

Fig. 3a and 3b show the forced frequency response of the UPD model at four different excitation levels, namely 0.96 N, 3.84 N, 9.6 N and 17 N and under a normal load of 960 N as shown in [12]. The excitation force is applied in the X direction at a node on the blade root as shown in Fig. 2b in a frequency range close to the first bending modes. The response is plotted for a node on the blade tips in the X direction, so to quantify the dynamic behaviour of the UPD model. The normal static pressure distribution on the contact surface was experimentally measured with pressure films, showing that a non-uniform pressure distribution occurred. This was directly interpolated and used in the simulations as in [12]. Friction coefficient  $\mu = 0.88$  and tangential,  $k_t$  and normal  $k_n$  contact stiffness of 44,000 N/mm<sup>3</sup> and 55,000 N/mm<sup>3</sup> respectively were used based on the recent measurement from the 1D friction rig [19].

Fig. 3a shows that there is a strong softening behaviour along with a 2 Hz frequency shift in the first in-phase bending mode when the excitation amplitude increases from 0.96 N to 17 N. The UPD still damps the dynamical response, since the receptance is decreased by 25% at the maximum force level. Fig. 3b shows, for the out-of-phase mode, the resonant receptance are reduced by more than 50% when the excitation force level increases from 0.96 N to 17 N. Such damping performance is better than that of the in-phase mode because the damper has a pure rolling motion during the in-phase vibration and a loss of contact takes place. This motion separates part of the contact surface which decreases the overall stiffness of the structure. This slightly reduces the effectiveness of the damper which is supposed to work when the contact interface is in contact.

To give more insight of such a different dynamic behaviour between the two modes, Fig. 4a show an example of the contact conditions at the UPD interfaces at the resonance frequency at the excitation level of 17 N. The majority of contact nodes are in a contact/separation condition (red) for the in-phase mode while the majority of contact nodes are in a stick condition (black) for the out-of-phase mode. The next section describes the uncertainty observed in the experimental measurements of contact parameters. This uncertainty should in fact be taken into account for more accurate simulations.

### 3. Uncertainty quantification of measured contact parameters

The dynamics simulations shown in the previous section are strongly dependent on the contact input parameters, namely the friction coefficient  $\mu$ , the normal and tangential contact stiffnesses  $k_n$  and  $k_t$ , and the pressure distribution at the contacting interfaces. These parameters strongly affect the dynamic response of the system, and hence their correct value should be used in simulations. However, their correct identification is challenging due to the high degree of uncertainty often observed in experiments. The aim of this section is to quantify this uncertainty by means of experimental measurements obtained from the high frequency friction rig built at Imperial.

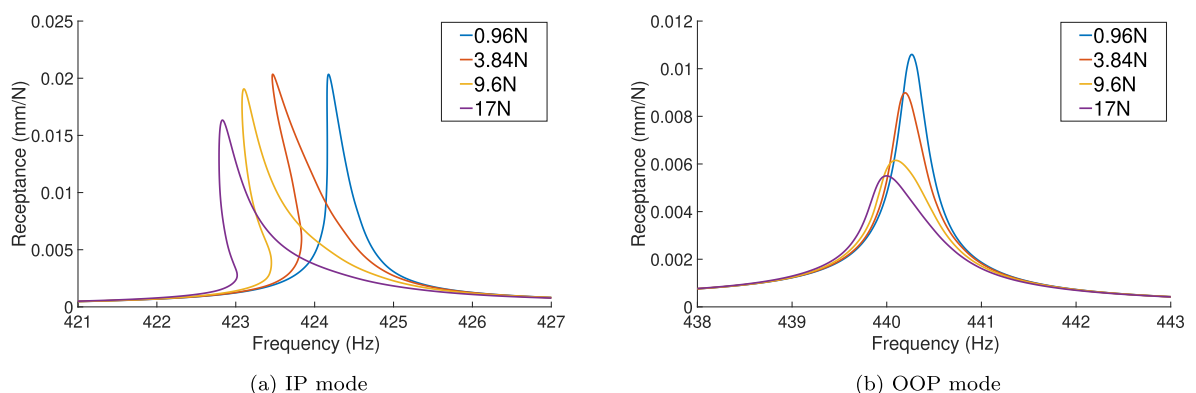


Fig. 3. Numerical simulations of the forced frequency response at different excitation levels.

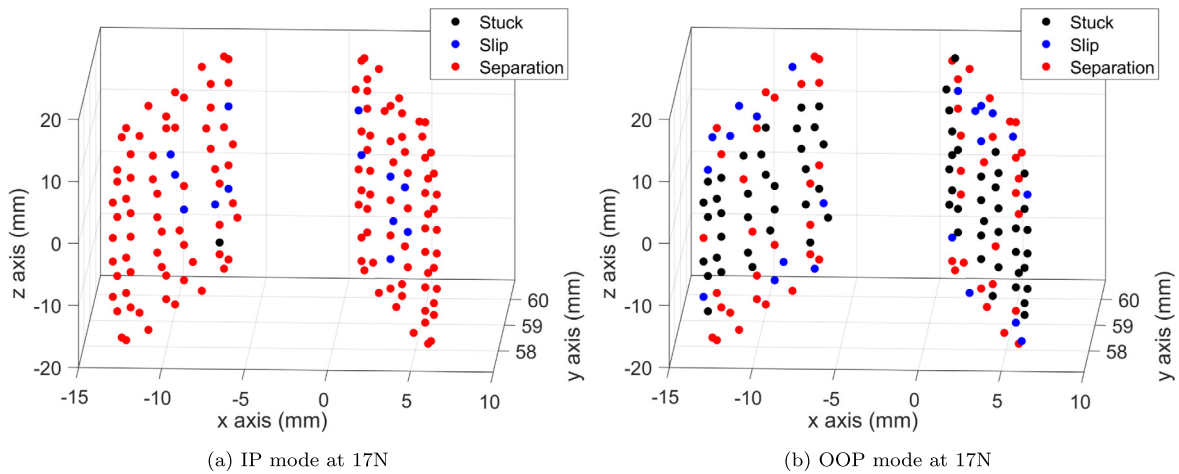


Fig. 4. An example of the resonant contact condition of interface nodes at the excitation level of 17 N.

### 3.1. The friction rig

The friction rig is shown in Fig. 5a and has been built to measure hysteresis loops, which provide the required input contact parameters used in dynamics simulations of turbomachinery systems with friction joints. The rig generates a high frequency sliding motion between a couple of specimens with a flat-on-flat contact, as those shown in Fig. 5b, and measures hysteresis loops as that of Fig. 1b. The relative displacement is measured by means of two Laser Doppler Vibrometers (LDVs), while the friction force is measured with force transducers. A continuous contact is ensured by applying a constant normal load by means of a pneumatic actuator. A more detailed description of the rig is provided in [19].

### 3.2. Experimental uncertainty of $\mu$ and $k_t$

Experimental hysteresis loops, such as those of Fig. 1b, are used to quantify the uncertainty in the contact parameters. In particular, only the uncertainty in friction coefficient and tangential contact stiffness has been quantified experimentally, while the normal load has been assumed to be constant during the experiments and the uncertainty in the normal contact stiffness has been considered equal to that of the tangential contact stiffness. It is also considered that the uncertainty from surface roughness is intrinsically included in the experimental uncertain distribution of these two parameters.

In previous research [16], fretting tests have been performed on a pair of stainless steel specimens (same material of the underplatform dampers used in this study) with a flat nominal area of contact of 1 mm<sup>2</sup>. The same data set has been re-analyzed here to quantify the uncertainties in the extracted parameters from different tests. Tests were performed at 60 N normal load, with an harmonic excitation of 100 Hz and a relative displacement of either 14  $\mu$ m (Tests 1 and 2 [16]) or 22  $\mu$ m (Tests 4 and 5 [16]). Each test lasted on average 5 h and hysteresis loops were recorded continuously. After each test, values of friction coefficient and tangential contact stiffness were extracted from each loop. The friction coefficient has been obtained by dividing the friction limit by the normal load, while the tangential contact stiffness has been obtained

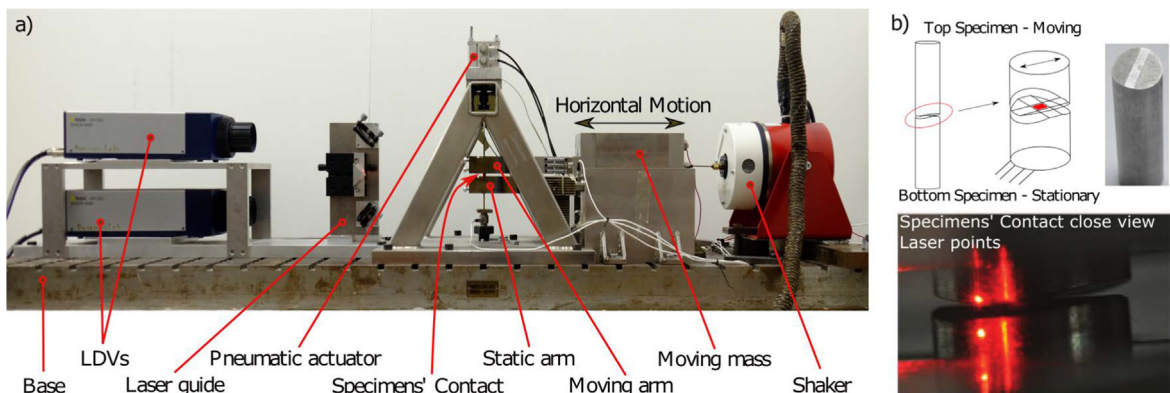
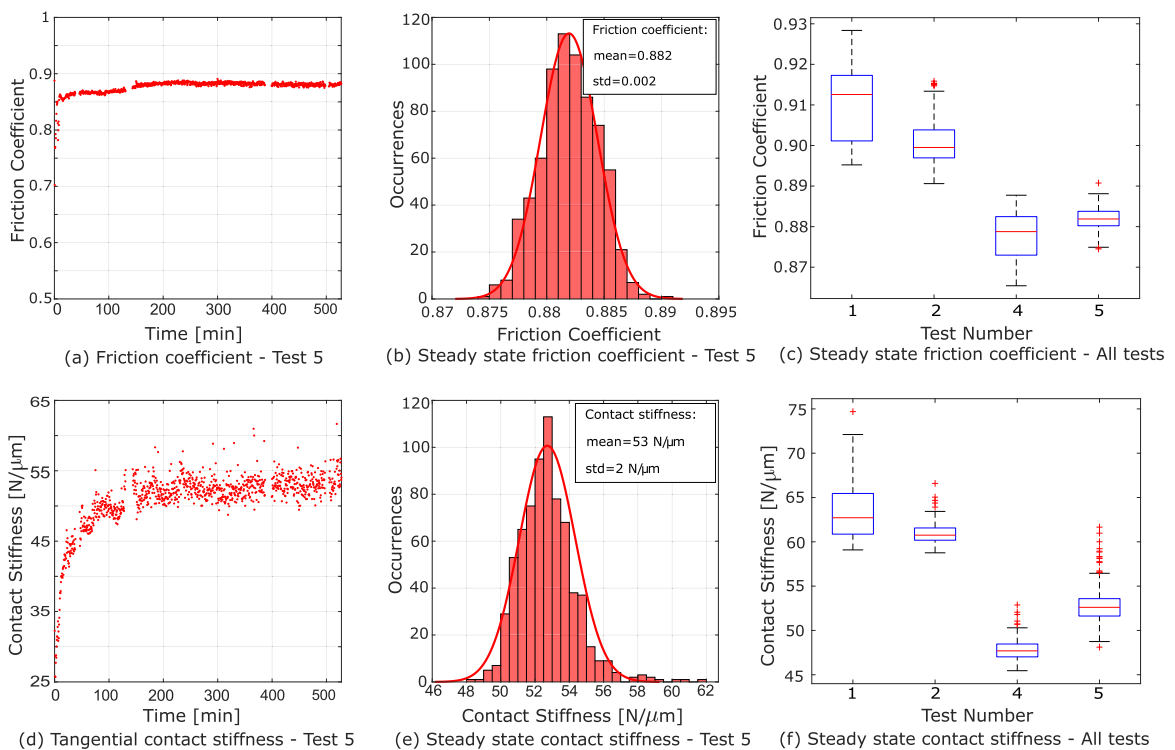


Fig. 5. The friction rig [19]: (a) Photo of the friction rig; (b) Specimens in contact.

from the slope of the stick portion of the hysteresis loop. It is worth noting that the friction coefficient obtained from the high frequency friction rig is the kinetic friction coefficient, and not the static friction coefficient that would be observed during the first loading only, and not during subsequent loadings. Since the harmonic balance method is used, the assumption of periodicity and steady-state is valid and therefore the static friction coefficient does not need to be accounted for as it does not appear in the steady-state vibration. The extraction of the parameters can be a source of uncertainty in addition to the uncertainty coming from the experiments. Therefore, a sensitivity study on the accuracy of the extraction was performed (not shown here for conciseness). The study showed that the relative standard deviation due to the extraction of the contact stiffness is below 0.9% while it is below the 0.03% for the friction coefficient. These values are both much lower than the standard deviation observed experimentally, as shown in the following.

Fig. 6a and d show the evolution of those two contact parameters over time for one test (the trend is the same for every test, and the reader is invited to refer to [16] for a full overview). Both parameters increase at the beginning of the test, with the friction coefficient reaching a steady state value of 0.88 within the first 10 min, while the tangential contact stiffness stabilises at around 53 N/μm after 200 min, with a larger uncertainty compared to that observed for the friction coefficient. Similar large values of friction coefficient (around 0.8) have also been measured from the high frequency friction rig at Politecnico di Torino within a Round-Robin test [52]. Fig. 6b and e show the distribution of the steady state values (all the values after 200 min) for friction coefficient and tangential contact stiffness respectively. Both parameters show a Gaussian distribution, with a relative standard deviation of 0.23% for the friction coefficient and 3.77% for the tangential contact stiffness. This variability is probably due to measurement noise coming from laser and load cell time signals. For this reason, the standard deviation observed in the contact stiffness is larger than that observed in the friction coefficient. In fact, for the extraction of the friction coefficient, only the friction force time signal is needed (plus the constant normal load). Instead, for the extraction of the contact stiffness the time signals of both the laser displacement and the friction force are required. The combination of the two results in greater noise from contact stiffness measurements than from friction coefficient measurements. However, it is to be noted that both standard deviations are still relatively low. This is because they relate to the steady state values of a single test, and do not include the variability observed within different tests, whose values are shown in Fig. 6c and f by means of boxplots of the steady state values. It is clear that the variability between different tests is larger than the standard deviation within the single tests, with differences in the mean values up to the 5% for the friction coefficient and up to the 30% for the contact stiffness. In fact, steady state values are included in the range 0.87–0.93 for the friction coefficient, and in the range 45–70 N/μm for the tangential contact stiffness. Although a reliable statistical analysis cannot be performed since the number of tests is low, the available data provide an estimation of the variability to be



**Fig. 6.** (a) Evolution in time of  $\mu$ ; (b) Statistical distribution of steady state  $\mu$  (values after 200 min); (c) Boxplots of steady state  $\mu$  for tests performed in [16]; (d) Evolution in time of  $k_t$ ; (e) Statistical distribution of steady state  $k_t$  (values after 200 min); (f) Boxplots of steady state  $k_t$  for tests performed in [16]; Tests 1 and 2 were conducted at a relative displacement of 14  $\mu\text{m}$ , while tests 4 and 5 at 22  $\mu\text{m}$ , as detailed in [16].

**Table 1**  
Uncertainty parameters used in this study.

$\mu$	mean: 0.88, relative std: 5%
$k_t$ [N/mm <sup>3</sup> ]	mean: 44000, relative std: 30%
$k_n$ [N/mm <sup>3</sup> ]	mean: 1.25*k <sub>t</sub> , relative std: 30%

expected for the friction coefficient and the tangential contact stiffness. This relatively large variability is probably due to the uncertainty induced by the different manufactured interfaces of the specimens and also to the assembly procedure. In addition, tests 1 and 2 were performed at a lower sliding amplitude than tests 4 and 5. It seems that this difference might affect the mean values of the contact parameters. Although this displacement dependency is not the focus of this study, its effect is accounted for by the chosen values of standard deviation.

Those experimental fretting tests have been in fact used to provide the mean and standard deviation values needed as input for the MCS. The chosen values are shown in Table 1. Please note that the contact stiffness is not expressed in [N/μm], but in [N/mm<sup>3</sup>] since an area-normalised stiffness is required in simulations. For the considered experimental tests [16], the average worn area of contact was of 1.2 mm<sup>2</sup>, which when divided by the mean of 53000 N/μm, led to a mean k<sub>t</sub> of 44000 N/mm<sup>3</sup>. In addition, the normal contact stiffness could not be extracted from the hysteresis loops, and it was assumed to be 1.25 larger than the tangential stiffness, as commonly suggested by contact mechanics studies [53]. Please notice that the contact stiffness is known to be normal load dependent [21]. However, in this uncertainty study, this effect was not included, thus keeping unchanged the values measured from the friction rig.

Finally, the statistical independence of friction coefficient and contact stiffness is investigated. Only the data in a steady-state regime has been used for the analysis in each test case. Firstly, both parameters can be represented as a bivariate random variable ( $X_\mu, X_{k_t}$ ) and could be approximated by a bivariate normal law. Secondly, the Pearson correlation coefficient  $\hat{r}$  defined as [54]:

$$\hat{r} = \frac{COV(X_\mu, X_{k_t})}{\sigma_\mu \sigma_{k_t}} \tag{3}$$

was then calculated for each case, and is always close to 0. Because the Pearson correlation coefficient is close to 0, and the bivariate random variable follows a bivariate normal law, it follows that the two statistical variables,  $\mu$  and  $k_t$ , are independent.

The values shown in Table 1 have been used for the uncertainty propagation analysis that is described in the next Section, from which dynamics predictions with confidence intervals were obtained and is discussed in Section 5.

#### 4. Uncertainty propagation

This section describes the methodology employed for the uncertainty propagation in the numerical model. As a reminder, the contact parameters, namely the friction coefficient  $\mu$  and the tangential contact stiffness  $k_t$  are considered as uncertain and can be described by normal laws whose characteristics are given in Table 1. Moreover, it has been demonstrated in Section 3.1 that they are also independent. Since the computational cost for statistical analysis associated to the UPD model is very high, Polynomial Chaos Expansion (PCE) is employed in the present study to model and propagate the uncertainty using the software OpenTURNS [55]. Using PCE, surrogate models can be generated which enable the simulation of the nonlinear dynamic system behaviour with very low computational cost. In the following, the mathematical aspects of PCE theory is shortly introduced as well as the strategy adopted for the construction of the learning sets to propagate uncertainty in the FRFs.

##### 4.1. Polynomial Chaos Expansion and Sobol indices: mathematical background

PCE is a stochastic approach that consists in projecting a stochastic solution on an orthogonal polynomial basis. This approach is based on the assumption that the uncertain parameters are described by a Probability Density Function (PDF). After computing the weighting coefficients, the PCE can be used as a surrogate model as it approximates the solution with a low computational cost. Moreover, the weighting coefficients are directly related to the Sobol indices, which are indices used to perform a sensitivity analysis and identify the most influential input parameters on the solution.

Let  $\mathbf{x} = (x_{k_t}, x_\mu)$  be the vector of the input variables and  $y$  the deterministic response of the system. The system response is parametrized with the phase rather than the frequency, more details will be given in the following section on this aspect. Hence  $y$  corresponds to the frequency or the receptance of the vibration of the system for one phase value. As the input vector  $\mathbf{x}$  is affected by uncertainty, it is represented by a random vector  $\mathbf{X}$ . Each random parameter is characterised by its PDF, here  $f_{k_t}(x_{k_t})$  for the tangential contact stiffness and  $f_\mu(x_\mu)$  for the friction coefficient. The PDF of the random variable  $\mathbf{X}$  is denoted  $f_{\mathbf{X}}(\mathbf{x})$  and is defined as  $f_{\mathbf{X}}(\mathbf{x}) = f_{k_t}(x_{k_t}) \times f_\mu(x_\mu)$ . The output is also a random variable denoted  $Y$ . According to the generalized polynomial chaos theory,  $Y$  can be expanded onto an orthogonal polynomial basis as follows [56,40]:

$$Y = \sum_{l=0}^{+\infty} a_l \Psi_l(\mathbf{X}) \tag{4}$$

where  $(a_l)$  are the unknown deterministic weighting coefficients, the  $(\Psi_l)$  are the multivariate orthogonal polynomials and  $l$  is the order of the polynomial  $\Psi_l$ . This series is convergent in the  $\mathcal{L}^2$  sense (i.e. the random vector is square-integrable), and is often called *Polynomial Chaos Expansion* (PCE) of  $Y$ . This series is normally truncated and only  $P$  terms are kept for numerical reasons.

The assumption of independence of the input random variables allows the overall PDF  $f_X$  via  $f_X(\mathbf{x}) = f_{k_t}(x_{k_t}) \times f_{\mu}(x_{\mu})$  to be computed. It is now possible to find a family of orthonormal polynomials with respect to each PDF to construct the  $(\Psi_l)$ .  $(\Phi_j^{(k_t)})$  and  $(\Phi_j^{(\mu)})$  are the polynomials family orthogonal with respect to  $f_{k_t}(x_{k_t})$  and  $f_{\mu}(x_{\mu})$  respectively, and where  $j$  denotes the order of the polynomial. For standard PDFs, the correspondence between the PDF and the orthonormal polynomial families is given by the Askey scheme [40]. As an example, Hermite polynomials are orthogonal with respect to the normal distribution, when Legendre polynomials are orthogonal with respect to the uniform distribution. The multi-variate polynomial family orthogonal to  $f_X(\mathbf{x})$  can be obtained by the tensorisation of  $(\Phi_j^{(k_t)})$  and  $(\Phi_j^{(\mu)})$ , which is equivalent to:

$$\Psi_l(\mathbf{X}) = \prod_{(i,j)} \Phi_i^{(k_t)}(x_{k_t}) \times \Phi_j^{(\mu)}(x_{\mu}) \tag{5}$$

$i + j = l$

where  $l$  is the order of the polynomial  $\Psi_l$ . Finally, only polynomials of order below the chaos order  $m$  are kept in the expansion (4) and only  $P$  terms remain in the expansion (4). The total number of terms in the series is  $P = \binom{m+d}{m}$ , where  $d$  is the dimension of the input space, equal to 2 here. The chaos order  $m$  is chosen based on a convergence study.

To determine the weighting coefficients  $(a_l)$ , intrusive or non-intrusive approaches might be used [57,46]. A non-intrusive regression approach is used here for its efficiency [46] and the coefficients  $(a_l)$  are determined by minimizing, in the least-square sense, the difference between  $N$  deterministic evaluations of the computationally expensive nonlinear dynamic model and its PCE evaluations. This set of  $N$  inputs and outputs is called the Design of Experiment (DoE). In the present study, a Latin Hypercube Sampling (LHS) is used to generate the input space [46].

In order to understand how sensitive the output  $Y$  is to the variance of the different input parameters, Sobol indices can be used. Sobol indices are sensitivity indicators that estimate the influence of the different input parameters as well as their coupling effects on the output variance. The PCE decomposition is directly related to the Sobol decomposition [46] and so, the Sobol indices can be deduced from the PCE coefficients  $(a_l)$ . If  $V(Y)$  is the variance of the output, it can be decomposed into [58]:

$$V(Y) = V_{\mu} + V_{k_t} + V_{\mu,k_t} \tag{6}$$

where  $V_{\mu} = V(E(Y|X_{\mu}))$ ,  $V_{k_t} = V(E(Y|X_{k_t}))$  and  $V_{\mu,k_t} = V(E(Y|X_{\mu}, X_{k_t})) - V_{\mu} - V_{k_t}$ , where  $E$  denotes the expectation. Finally, the first order Sobol indices are defined as [58]:

$$S_{\mu} = \frac{V_{\mu}}{V(Y)} \quad S_{k_t} = \frac{V_{k_t}}{V(Y)} \tag{7}$$

and second order index is defined as:

$$S_{\mu,k_t} = \frac{V_{\mu,k_t}}{V(Y)} \tag{8}$$

Sobol indices are good indicators to describe the sensitivity of a function to its input parameters and their coupling effects. If the Sobol index  $S_i$  of a variable  $x_i$  is low (i.e. close to 0), then the variable  $x_i$  has a low influence on  $Y$ . If the Sobol index is high (i.e. close to 1), then the variable  $x_i$  has a strong influence on  $Y$ . In this study, the variable  $Y$  is either the amplitude or the frequency of vibration of the structure. First order indices give the influence of each input parameter taken alone, and higher order indices describe the influence of the interaction between the different parameters on the variance of the output variable.

#### 4.2. PCE for nonlinear FRFs

The PCE is used in the present study to construct a meta-model of the nonlinear FRF response of the system. Because of the nonlinear aspect of the system, several dynamic solutions may exist for one frequency, as shown for example in Fig. 3a where a softening effect leads to three different solutions in the range of frequencies between 423–424 Hz. To overcome this issue, the phase can be used to propagate the uncertainty [42,41] rather than the frequency. The phase refers here to the phase angle between the shaker excitation and the fundamental of the output displacements which is unique for each point on the FRF as illustrated in the 3D plot in Fig. 7, where the frequency, the phase and the receptance of a FRF are given for the mean value of each random parameter. As it can be seen, the phase is strictly increasing over a FRF, so each point of the FRF is

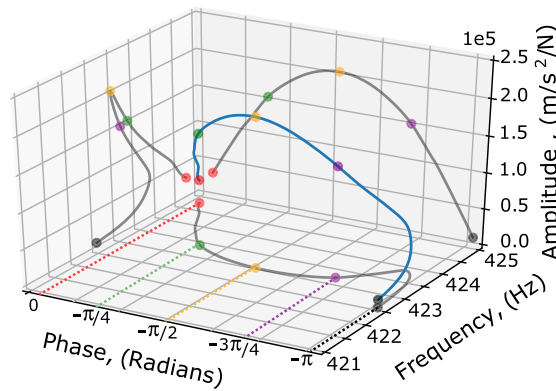


Fig. 7. An example of Phase-Frequency-Amplitude 3D graph of a IP mode FRF.

characterised by a unique phase. So, for one phase value, there is a unique frequency and a unique receptance. Hence, the phase is used as the deterministic parameter, and each FRF is decomposed in the combination of a phase frequency function and a phase receptance function. For each phase value, two PCEs are constructed: one for the frequency and one for the receptance, where both the friction coefficient  $\mu$  and the tangential contact stiffness  $k_t$  are uncertain. In other words, one DoE has the values of  $(\mu, k_t)$  as input, and the values of the frequency (or the receptance) for one particular phase value as output. The other reason is that PCE usually has bad convergence properties for discontinuous function. With this parameterization, PCE can be constructed only on continuous functions to avoid this issue [41,59]. Based on this approach, the PCE can then be constructed as outlined in the next section.

## 5. Numerical uncertainty propagation and validation against experiments

In this section, the PCE meta-models are constructed and numerically validated. They are also experimentally validated against data from the UPD rig, and are used to replicate the nonlinear dynamic behaviour of the system and to investigate the influence of the different contact parameters on the uncertainty.

### 5.1. Numerical uncertainty propagation

As previously explained, two uncertain parameters are considered here, the friction coefficient  $\mu$  and the tangential contact stiffness  $k_t$ . Based on the experimental data from Section 3, they are both described by a normal law whose parameters are given in Table 1. A non-intrusive approach is used for the PCE construction as described in Section 4, and the input set is generated by considering a LHS of 50 samples of  $(\mu, k_t)$ . Then, for each couple  $(\mu, k_t)$  of the LHS, the FRF of the system over the two frequency ranges of first and second modes are computed with the MHBM, as described in Section 2.1. Four different constant shaker force amplitudes [0.96, 3.84, 9.6, 17] N are used to study the nonlinearity in the system at different levels, leading to a total of 200 nonlinear simulations. The computation of a nonlinear FRF with the computationally expensive nonlinear dynamic model takes about 45 min, so the 200 simulations represent about 150 h. Each FRF is then decomposed into a phase receptance response and a phase frequency response for the PCE construction. As an example, the FRFs for both the in-phase and out-of-phase modes for the 17 N case are given Fig. 8c and f, respectively. The corresponding phase receptance response and the phase frequency response decomposition are given in Figs. 8(a,b) for the in-phase mode and in Figs. 8 (d,e) for the out-of-phase mode.

The uncertainty induced by the contact parameters has large effects on both modes. For example, the resonance receptance of the in-phase mode varies by  $\pm 20\%$  and the frequency is shifted up to 7 Hz. Considering the out-of-phase mode, the peak at resonance can be shifted up to 1.5 Hz and the receptance varies by  $\pm 30\%$ . For lower levels of excitation amplitude, the effects of the uncertain parameters are similar and are not presented here for the sake of brevity.

For each mode and for each loading case two PCEs are constructed for each phase value, as explained previously in Section 4.2. Thus, each FRF is decomposed into a phase frequency response and a phase receptance response, and for each phase value two PCEs are constructed: one for the receptance and one for the frequency [42]. The PCE order was determined based on a convergence study and is chosen equal to 4 in all cases. Validation was done by comparing the PCE predictions at learning points and as the PCE is not an interpolation method, this approach can stand for validation. The validation showed that the PCE predictions were within 1% from the reference values, providing confidence that the trained PCE models were able to accurately replicate the nonlinear dynamic response of the system under investigation.

The validated PCE models were then used to predict the nonlinear FRF of the system, and so to predict the dynamics of the blades taking into consideration the uncertainty related to the friction coefficient  $\mu$  and the tangential contact stiffness  $k_t$  at a significantly reduced numerical cost. A Monte Carlo (MC) simulation with 1000 samples was computed with the different PCE (i.e. for each phase value) to generate the corresponding phase receptance and phase frequency responses. Fig. 9 shows

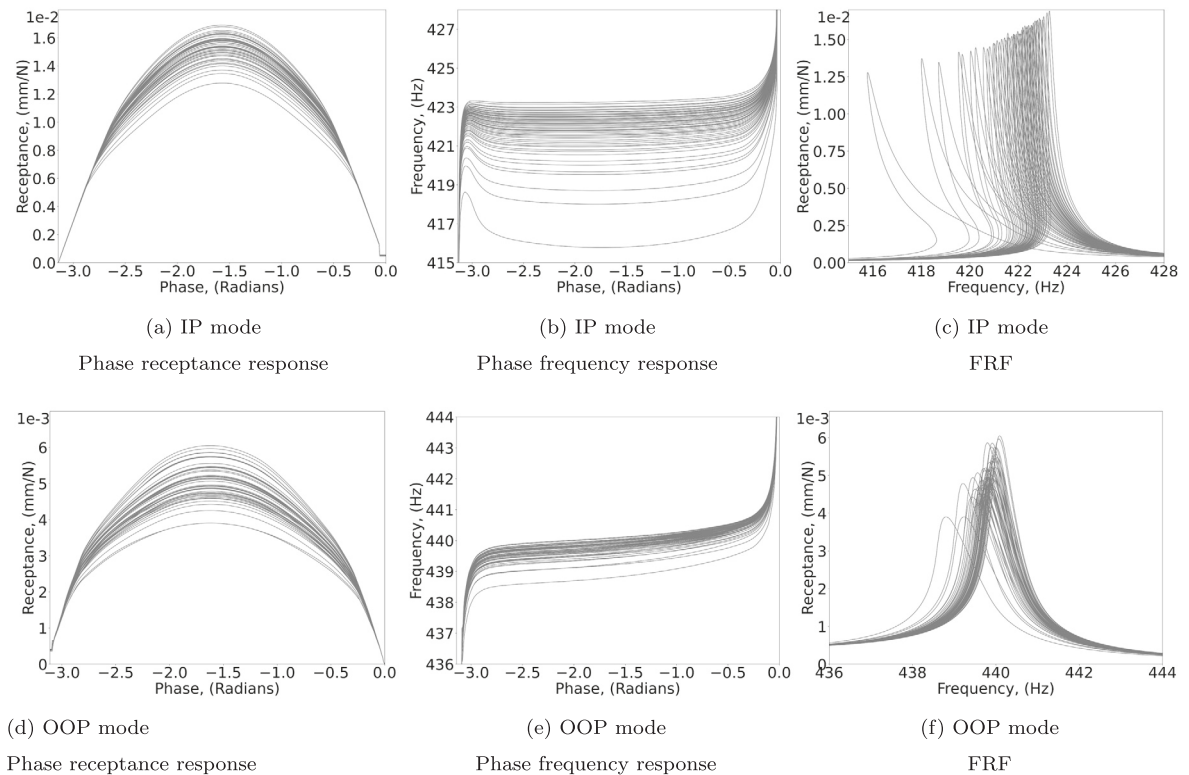


**Fig. 8.** Monte Carlo simulation phase receptance responses (a,d), phase frequency responses (b,e) and frequency response functions (c,f) of the in-phase (a,b,c) and out-of-phase (d,e,f) modes generated from the LHS of 100 samples of  $(\mu, k_t)$ .

the resulting vibration response for the in- and out-of-phase modes at 17 N as an example. The phase receptance and phase frequency responses are shown in Fig. 9d) and (b,e) respectively, where the blue line corresponds to the average at each phase point, and the 90% confidence band is indicated by the red lines. For each response, the FRF is reconstructed and is shown in Fig. 9(c,f), where the average is determined for each phase value.

From these results, the impact of the uncertainty of the contact parameters on the dynamic response can be assessed. For the IP mode, the impact of the uncertainty is maximum at the resonance, since it is where the maximum of variation is observed in Fig. 9(a). Indeed, at the resonance the receptance can vary by  $\pm 20\%$ , while away from resonance, the variability decreases and drops to zero at the extreme frequency ranges. Considering the frequency (see Fig. 9b), the largest dispersion is observed between  $-2.7$  rad and  $-0.2$  rad further highlighting the stronger effect the uncertainties have around the resonance. When the phase increases, the dispersion decreases and tends to be null for a 0 rad phase. Considering the OOP mode, the receptance can vary up to  $\pm 30\%$  at resonance, while away from resonance, the variability decreases very slowly and only drops to zero at the extreme frequency ranges, meaning that the uncertainty related to the contact has no impact on the dynamic of the system far away from resonance. Considering the frequency for the out-of-phase mode (see Fig. 9e), the dispersion is lower than compared to that for the IP mode.

In order to evaluate the impact of the excitation level, the evolution of the distribution of the frequencies and amplitudes at the resonance (i.e. when the phase is equal to  $-\pi/2$ ) is studied for both modes leading to the boxplots in Fig. 10. The green dotted lines stands for the average value and the yellow one for the median value.

In all cases, the frequencies and amplitudes at resonance decrease when the excitation amplitude increases. At very low excitation levels (i.e. for the 0.96 N case), the damper is always fully stuck and there is no energy dissipation, which explains why the uncertainty of the amplitude is very low and not impacted by the variability in the contact parameters. For the frequency, for the IP mode, the dispersion becomes larger when the excitation amplitude increases. At low level of excitation, the frequency shift is due to the variation of the tangential contact stiffness  $k_t$  which affects the stuck regions of the hysteresis loops and consequently has an impact on the response when the interface is stuck. In addition, by changing the excitation from 0.96 N to 17 N, the receptance reduces by 25% in average for the IP mode, and by 50% in average for the OOP mode.

### 5.2. Comparison against experimental data

In this section, the constructed PCE models are compared with existing experimental data from the UPD test shown in Fig. 2a [12]. The measurement setup of this test rig is briefly reminded to show how the experimental data is collected. After

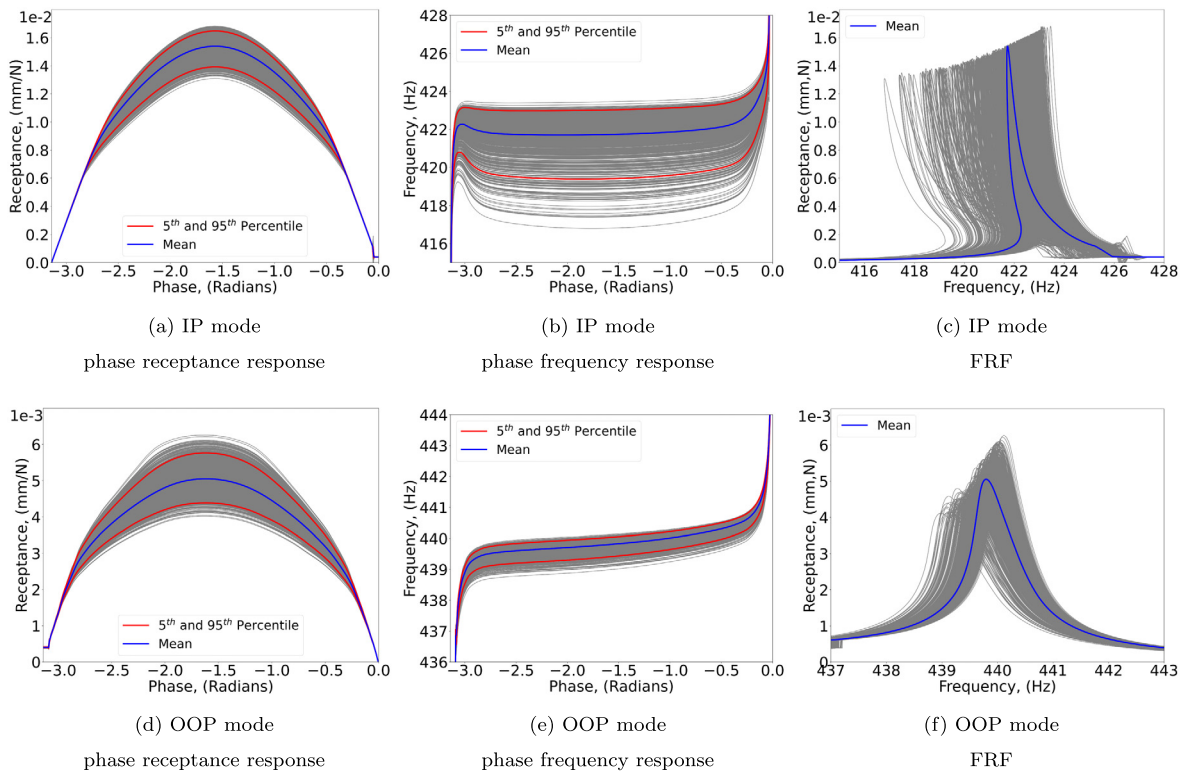


**Fig. 9.** PCE simulation phase receptance responses (a,d), phase frequency responses (b,e) and frequency response functions (c,f) obtained from MCS simulations for the IP mode (a,b,c) and the OOP mode (d,e,f) for the 17 N shaker force amplitude - Average values (blue line), 90% confidence band (red lines). For interpretation of the references to colour in this figure legend, the reader is referred to the web version of this article.

that, two sets of experimental data from the rig are shown and compared to the statistic results generated from the PCE models.

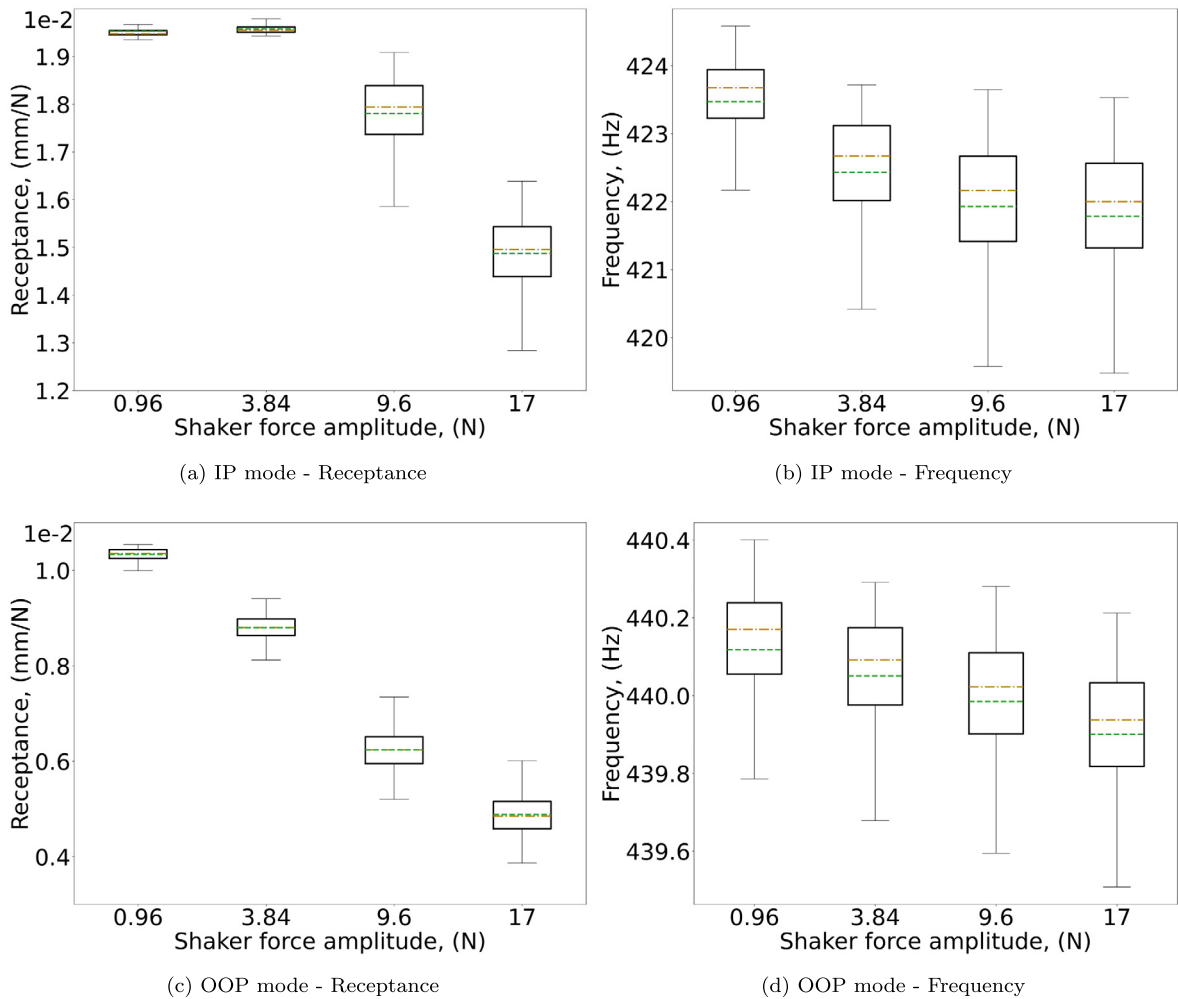
### 5.2.1. UPD test rig measurement setup

Fig. 2a shows the measurement setup of UPD test rig [12] used to measure the nonlinear dynamic response of two static blades equipped with one UPD. The blades are clamped tightly to a 2000 kg inertia block via an hydraulic vice capable of 200 kN clamping force. The centrifugal loading is simulated via a pulley system, which was kept the load constant at 960 N to ensure a good conformity at the contact interface. The forcing excitation is provided by an electrodynamic shaker, which is attached below the platform in the same position highlighted in the FE model in Fig. 2b. A stepped sine test with force control was performed with a Data Physics SignalCalc ACE card around each resonance at various levels of excitation, from 0.01 N to 17 N. The response was measured with two non-contacting laser Doppler vibrometers (LDV) focused near the tip of each blade. A comparison of experimental data with deterministic simulations showed a reasonable good agreement, but some discrepancies were observed that could not easily be explained [12]. Here the comparison with the stochastic simulations is presented.

### 5.2.2. PCE vs Experimental data

The UPD model presented in Section 2.3 was updated to ensure that its linear response was similar to that of the experimental data sets. The model was updated by identifying the linear modal damping ratio of the UPD model from the experimental data sets at 0.096 N by using the Half-Power bandwidth method. The linear modal damping ratio identified for the IP mode is 0.063% and for the OOP mode is 0.048%, which are 2.51 times and 1.89 times higher than the damping ratios used in the initial UPD model.

While the comparison of amplitude at high excitation levels is presented in the following, the frequency phase plots are not compared in this paper because the linear natural frequencies for this UPD model have not been updated making such a comparison not very meaningful. Fig. 11 shows the comparison of the receptance between experimental data and the updated PCE models for both in-phase mode and out-of-phase mode separately at four excitation force levels, namely 0.96 N, 3.84 N, 9.6 N and 17 N. Two sets of experimental data are used to represent the experimental measurement for each excitation level, plotted respectively with yellow and black dots.



**Fig. 10.** PCE predictions: statistical distribution of the receptance (a,c) and the frequency (b,d) of the IP (a,b) and OOP (c,d) modes at the resonance for different excitation amplitudes - Average value (green dotted line) and median value (gold yellow line). For interpretation of the references to colour in this figure legend, the reader is referred to the web version of this article.

For the IP mode, the unstable part of the experimental response could not be captured because of the softening effects in the IP forced response. Amplitudes of the two experimental FRFs differ up to the 20% in the resonance regions at low excitation levels. This is a larger variability than that predicted by PCE model. Instead, at higher excitation at 3.84 N, 9.6 N and 17 N, the 90% confidence bands determined from PCE models are able to include the two sets of experimental data. It is clear that, at 0.96 N, the PCE does not capture well the experimental data. Such a disagreement can be due to the uncertainties related to the variation in the normal load across the interface. In fact, the IP mode is dominated by contact separation conditions (shown in Fig. 4a) and therefore is more sensitive to the variation in the normal load.

For the OOP mode, the majority of the experimental data points lie within the 90% confidence interval identified from the PCE model especially at 3.84 N to 17 N. It means that the constructed PCE models including the uncertainties in  $\mu$  and  $k_t$  can effectively capture the existing experimental data. One can also observe that the discrepancy between the two experimental data sets increases over the four force levels. This is consistent with the variation of predicted confidence intervals from the PCE models. Off resonance, the experimental data mostly overlapped in a similar manner to the PCE predictions.

The agreement between the uncertainty bands predicted from PCEs and sparse experimental FRFs suggests that the distribution of contact parameters was properly quantified from the experiments through the high frequency friction rig described in Section 3.1 and should not be ignored in the simulations since it leads to variations in the nonlinear dynamic response.

Overall, the results from the PCE models capture the majority of the experimental data points across different excitation levels well, indicating that the constructed PCEs can be used to quantify the uncertainties due to friction parameters in the nonlinear dynamics of turbine blades and can enable other statistical investigations, such as the Sobol analysis that is presented in the next section.

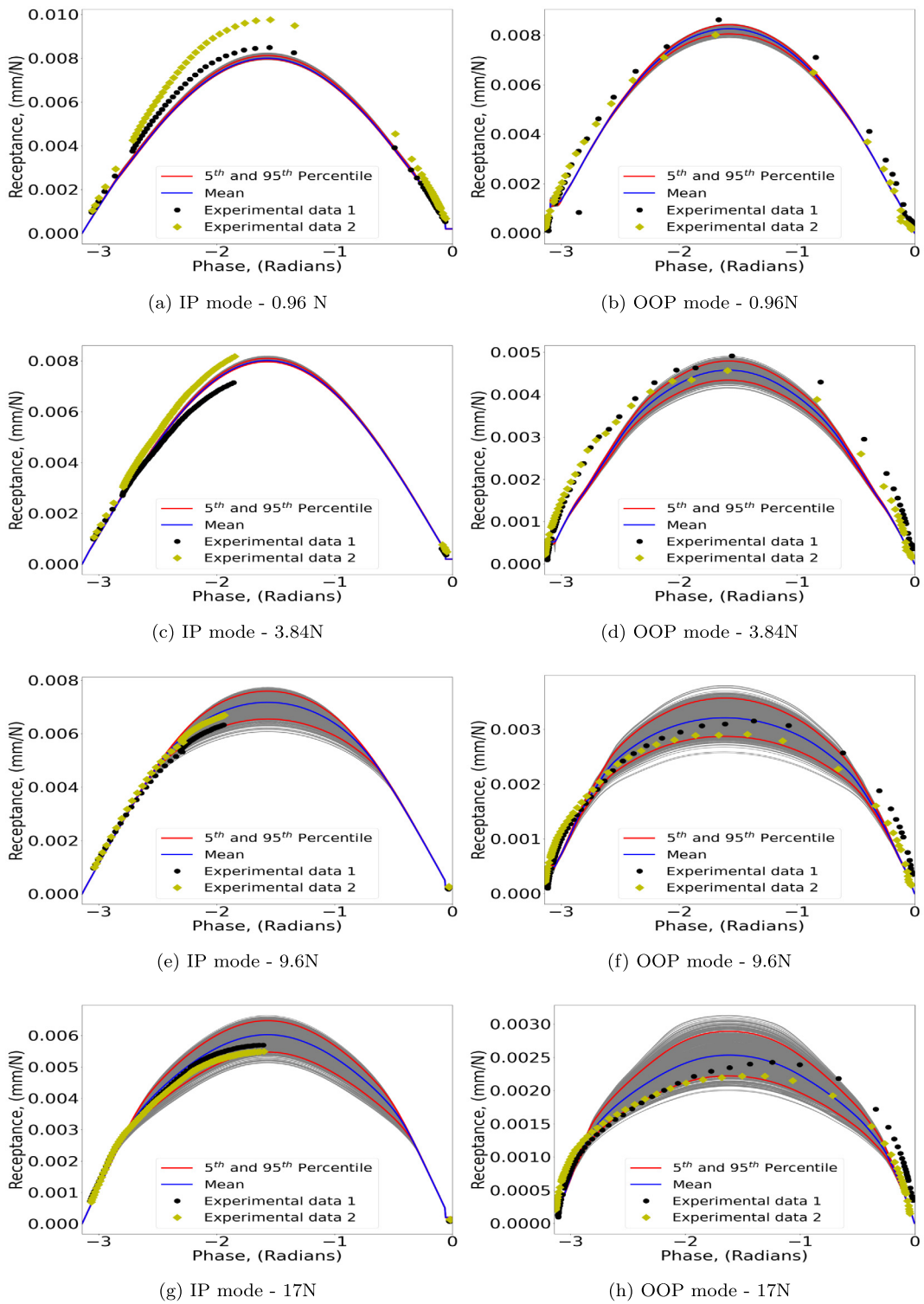


Fig. 11. Comparison of amplitude response from the updated PCE models and experimental data from the UPD rig.

### 6. Sobol analysis

The PCE can be further exploited by performing a Sobol analysis to study the influence of the contact parameters on the variance of vibration amplitude and frequency. As mentioned in Section 4.1, the Sobol analysis is a global variance based sensitivity analysis which decomposes the variance of the output of the model or system into fractions, called Sobol indices, that can be attributed to inputs or sets of inputs [60]. When the Sobol index of an uncertain parameter is close to 1, the parameter has a high influence on the output, while when the Sobol index is close to 0, the parameter has a low influence. In this way, the influence of the variability friction coefficient and contact stiffness on the FRFs can be quantified and analysed to get insights into the behaviour of the structure. It is worth highlighting here the difference between Sobol indices and more classical sensitivity analysis based on a perturbation method as in [14]. Sobol indices are able to take into account the interactions between different input parameters, which is not the case for the perturbation method. Moreover, the Sobol indices are directly related to the distributions that characterises the different input parameters (as they depend on the PCE decomposition), whereas the perturbation method is not. For these different reasons, only a Sobol analysis is considered here.

In this study, the uncertain parameters ( $\mu$  and  $k_t$ ) are considered for the Sobol analysis by using the Python library OpenTURNS [55]. Their Sobol indices have been determined directly from the PCE decomposition to study their influence on the FRFs, in terms of vibration amplitude and frequency. In particular, the first order Sobol indices as well as the Sobol coupling indices were computed for the in-phase and the out-of-phase modes at each phase value, for four excitation levels: 0.96 N, 3.84 N, 9.6 N and 17 N. The results for the 9.6 N case are similar to the 17 N case, and so are not presented in details in the following for the sake of consistency.

#### 6.1. Effect of contact parameters on the variance of the vibration amplitude

This section focuses on the Sobol indices evaluated for the vibration amplitude. The Sobol for the two modes behave differently, as described in the following:

- IP Mode – low percentage of contact points in slip condition:

Figs. 12(a-c) show the Sobol indices for the IP mode and Figs. 12(d-f) include the distribution percentage envelopes of the contact conditions of the 100 samples used for the PCE construction (i.e. % of contact points in stuck, slip and separation) at each phase value. This allows to link the contact status to the Sobol indices at the different phase values.

Fig. 12d shows that the percentage of contact points in slip condition is almost null for the 0.96 N loading case. This low slip percentage is reflected in the Sobol indices (see Figs. 12a), since the Sobol index  $\mu$  is null over most of the phase range (i.e.  $\mu$  has a very low influence on the variance of the amplitude), while  $k_t$  causes most of the variability in the amplitude.

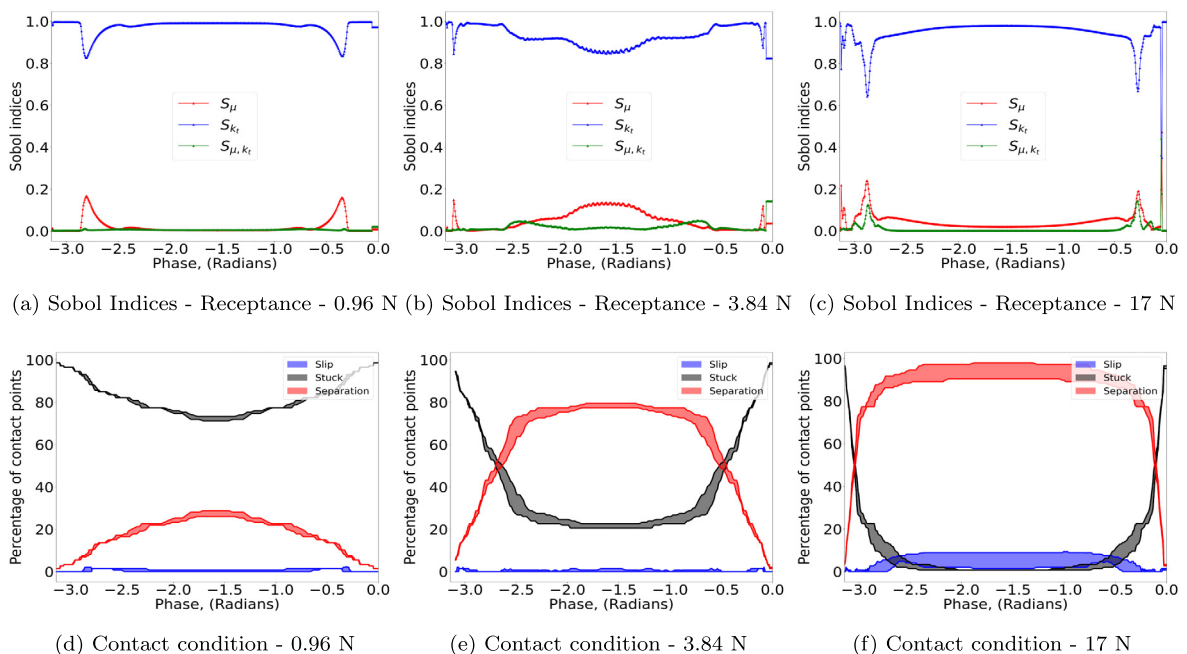


Fig. 12. IP mode: Sobol indices of vibration amplitude at different excitation levels: (a) 0.96 N; (b) 3.84 N; (c) 17 N; Distribution of the contact conditions: (d) 0.96 N; (e) 3.84 N; (f) 17 N.

It is in fact expected that the friction coefficient does not play a role since most of the contact points are in stuck conditions and hence do not activate the friction coefficient. However, tiny peaks are observable in the Sobol index of  $\mu$  at  $-2.7$  rad and  $-0.4$  rad, which correspond to peaks in the slip contact conditions (see Fig. 12d). It is interesting to note that the separation contact condition does not seem to affect the Sobol index behaviour, although it increases at resonance ( $-1.5$  rad) up to the 30%.

Low values in the Sobol index of  $\mu$  are also observed for the 3.84 N and 17 N loading cases (see Fig. 12b-c). However, in those cases it is more difficult to link the Sobol indices behaviours to the contact conditions. Still, it can be concluded that the observed low slip conditions result in a large influence of the contact stiffness  $k_t$  on the results, rather than the friction coefficient  $\mu$ , thus explaining the low Sobol index of  $\mu$  values. For those two loading cases, some coupling is also observed (two peaks in the green plots in Figs. 12b-c), indicating that microslip probably occurs at those phases, since during microslip the contact is determined by both the friction coefficient  $\mu$  and the contact stiffness  $k_t$ . Finally, it seems clear that the Sobol are unaffected by the separation contact condition, which, for the 17 N case, is appears in up to 90% of the contact nodes (see Fig. 12f) without although affecting the Sobol indices.

- OOP Mode – larger percentage of contact points in slip condition and microslip:

With regards to the OOP mode, a higher percentage of contact nodes are in the slip condition compared to the IP mode (see Fig. 13d-f). This larger slip percentage is reflected in the Sobol index of  $\mu$ , which is larger for all the loading cases. For each case, one can see strong variations of the Sobol indices far from resonance. These strong variations are always observed for phase values where the output variance is almost null, shown by comparisons with Fig. 11. As a consequence, the reliability of the Sobol indices for these phase values is reduced due to the poor statistical significance given by the low variance of the output. As soon as the variance in the amplitude for both modes increases as shown in Fig. 10c, the Sobol indices become more reliable. Moreover, when the excitation level is higher, the variance in the amplitude expands toward phases further away from the resonance phase, as shown in Fig. 11h compared to Fig. 11d where a large variance in the amplitude only appear close to the resonance. Consequently, for the 3.84 N loading case, the Sobol indices experience some instability at phases away from resonance, while for the 17 N case they are stable even at phases away from resonance. The first order Sobol index of the friction coefficient increases from 0 to 0.4 at the same phases where an increase in the variance amplitude is observed in Fig. 11d. This behaviour is again probably driven by slip conditions as shown in Figs. 13e-f. It is also interesting to note that the Sobol coupling term between  $\mu$  and  $k_t$  is null over the whole frequency range, suggesting that the coupling between the two parameters is negligible for this mode.

### 6.2. Effect of contact parameters on the variance of the frequency

This section shows the results for the Sobol indices evaluated for the frequency. Figs. 14a-b show the Sobol indices for the frequencies evaluated for the 3.84 N case for IP mode and OOP mode respectively. It is clear that the frequency is only influ-

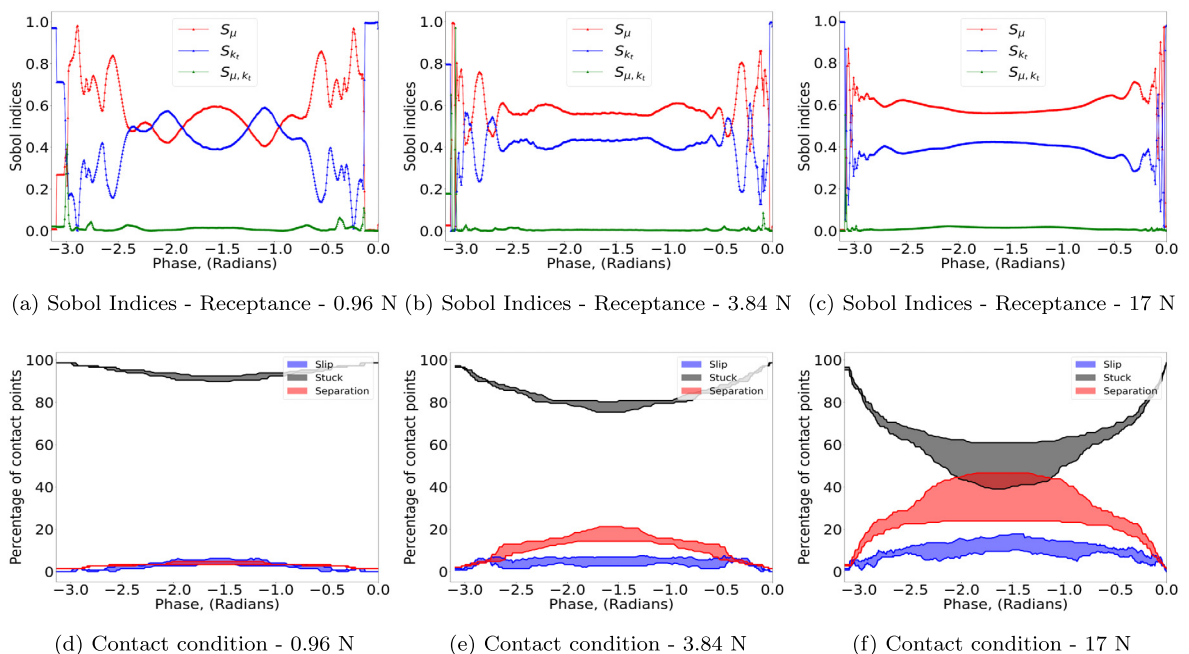


Fig. 13. OOP mode: Sobol indices of vibration amplitude at different excitation levels: (a) 0.96 N; (b) 3.84 N; (c) 17 N; Distribution of the contact conditions: (d) 0.96 N; (e) 3.84 N; (f) 17 N.

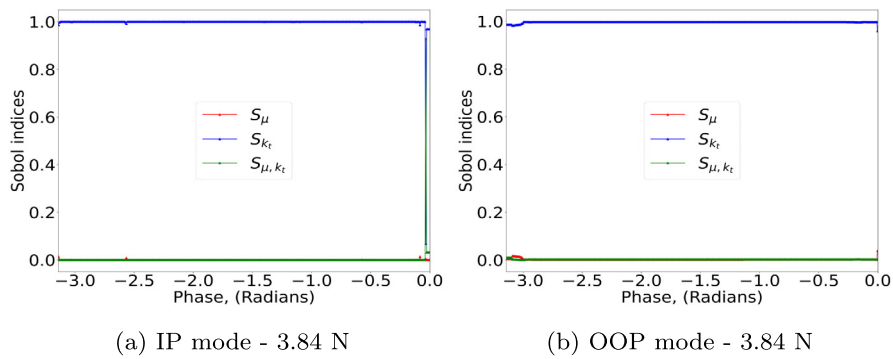


Fig. 14. Sobol indices of frequency for the 3.84 N loading case: (a) IP mode; (b) OOP mode.

enced by the contact stiffness, while changes in the friction coefficient do not affect the frequency. This behaviour is the same for all the other loading cases, and that is why they are not presented. This strong frequency dependency on the contact stiffness is probably due to the low percentage of contact nodes in slip conditions, which is always below the 15% for all cases as shown in Fig. 12d-f.

### 6.3. Summary

The use of Sobol indices confirmed the information obtained from the analysis of the contact conditions. These information can help engineers in better understanding the dynamic behaviour of systems with friction contacts. Results have shown that when the contact is fully stuck, the contact stiffness has a maximum influence, as can be expected, while the friction coefficient has a Sobol index close to zero. However, when the amount of contact nodes in slip condition increase, the Sobol index of  $\mu$  increases especially for the amplitude. This indicates a strong influence of the friction coefficient on the amplitude and its variance during slip. However, the frequency is still unaffected by the slip contact conditions, probably because for the analysed case, the slip contact conditions were relatively low. It is also worth noticing that the reliability of the Sobol indices are strongly dependent on the variance of the output. When the variance is low, the Sobol indices are unstable, and therefore not reliable. Sobol can provide reliable data only when the variance in the output is large enough, so that the Sobol indices reach stability. Still, Sobol indices represent an easy tool to implement in order to validate and provide useful insights on a structure, with a relatively cheap computing cost.

## 7. Conclusions

This work quantified the effect of the variability in friction coefficient and contact stiffness on the dynamic response of turbine blades equipped with underplatform dampers. The objective of this quantification was to obtain uncertainty bands in the dynamic response, and also to identify the role and the contribution of each parameter to the same response. In order to compute the uncertainty bands, numerical simulations were performed that combined a state-of-the-art nonlinear solver based on the multi-harmonic balance method with surrogate models based on the Polynomial Chaos theory. The normal distributions of friction coefficient and contact stiffness were identified based on existing experimental data, with relative standard deviations below the 5% for the friction coefficient and below the 30% for the contact stiffness. These distributions were then used to generate a Latin Hypercube sampling space for high fidelity simulations, and to define the polynomial basis of the Polynomial Chaos Expansion surrogate models. The surrogate models were used at nearly no numerical cost to generate numerical simulations for a wider range of friction coefficients and contact stiffness combinations, leading to Monte Carlo based uncertainty bands in the dynamic response. The confidence bands thus obtained were compared to sparse experimental data from an underplatform damper rig indicating some agreement between prediction and simulation. The results clearly show that the uncertainty in the contact parameters cannot be neglected in simulations, since it leads to large variations in the dynamic response.

The PCE models were then used to perform a Sobol analysis in order to rank the sensitivity of each uncertain parameter to the variability of the nonlinear dynamic response. The evolution of the Sobol indices of the contact parameters over the phase was studied, establishing a correlation between the contact conditions and the greater influence of contact stiffness compared to the friction coefficient. The novel use of the Sobol indices for nonlinear dynamic analysis has shown a promising capability in capturing contact nonlinear behaviours. Hence, this study shows that these statistical tools can be successfully used for nonlinear dynamics response predictions of systems with friction to obtain insights into the complex physics of the vibration.

## CRediT authorship contribution statement

**J. Yuan:** Conceptualization, Methodology, Writing - original draft, Project administration. **A. Fantetti:** Conceptualization, Methodology, Writing - original draft. **E. Denimal:** Conceptualization, Methodology, Writing-original draft. **S. Bhatnagar:** Software, Writing - original draft. **L.Pesaresi:** Writing - review & editing. **C. Schwingshackl:** Writing - review & editing. **L. Salles:** Writing - review & editing, Supervision.

## Declaration of Competing Interest

The authors declare that they have no known competing financial interests or personal relationships that could have appeared to influence the work reported in this paper.

## Acknowledgements

The authors would like to acknowledge the support of Rolls-Royce plc through the Vibration University Technology Centre (UTC) at Imperial College London, UK. J. Yuan and C. Schwingshackl have received funding from EPSRC through SYSDY-MATS WP3 project (EP/R032793). E. Denimal and L. Salles have received funding from Rolls-Royce and the EPSRC under the Prosperity Partnership Grant CornerStone (EP/R004951/1). A. Fantetti has received funding from the European Union's Horizon 2020 research and innovation program under the Marie Skłodowska-Curie grant agreement No 721865, project acronym "EXPERTISE".

## References

- [1] E. Seinturier, Forced response computation for bladed disks industrial practices and advanced methods, *Lecture Series-von Karman Institute Fluid Dyn.* 2 (2007) 5.
- [2] D. Ewins, Control of vibration and resonance in aero engines and rotating machinery—an overview, *Int. J. Press. Vessels Pip.* 87 (9) (2010) 504–510.
- [3] L.M. Amoo, On the design and structural analysis of jet engine fan blade structures, *Prog. Aerosp. Sci.* 60 (2013) 1–11.
- [4] M. Krack, L. Salles, F. Thouverez, Vibration prediction of bladed disks coupled by friction joints, *Arch. Comput. Methods Eng.* 24 (2016) 589–636.
- [5] J.H. Griffin, Friction Damping of Resonant Stresses in Gas Turbine Engine Airfoils, *J. Eng. Power* 102 (2) (1980) 329–333.
- [6] K.Y. Sanliturk, M. Imregun, D.J. Ewins, Harmonic Balance Vibration Analysis of Turbine Blades With Friction Dampers, *J. Vib. Acoust.* 119 (1) (1997) 96–103.
- [7] L. Gaul, J. Lenz, Nonlinear dynamics of structures assembled by bolted joints, *Acta Mech.* 125 (1–4) (1997) 169–181.
- [8] R. Lacayo, L. Pesaresi, J. Groß, D. Fochler, J. Armand, L. Salles, C. Schwingshackl, M. Allen, M. Brake, Nonlinear modeling of structures with bolted joints: a comparison of two approaches based on a time-domain and frequency-domain solver, *Mech. Syst. Signal Process.* 114 (2019) 413–438.
- [9] D.J. Segalman, A Four-Parameter Iwan Model for Lap-Type Joints, *J. Appl. Mech.* 72 (5) (2005) 752–760.
- [10] D.J. Segalman, Modelling joint friction in structural dynamics, *Struct. Control Health Monitor.* 13 (1) (2006) 430–453.
- [11] E. Petrov, A high-accuracy model reduction for analysis of nonlinear vibrations in structures with contact interfaces, *J. Eng. Gas Turbines Power* 133 (10) (2011) 102503.
- [12] L. Pesaresi, L. Salles, A. Jones, J.S. Green, C.W. Schwingshackl, Modelling the nonlinear behaviour of an underplatform damper test rig for turbine applications, *Mech. Syst. Signal Process.* 85 (2017) 662–679.
- [13] M. Krack, L. Panning, J. Wallaschek, C. Siewert, A. Hartung, Robust design of friction interfaces of bladed disks with respect to parameter uncertainties, in: *ASME Turbo Expo 2012: Turbine Technical Conference and Exposition, American Society of Mechanical Engineers Digital Collection*, 2012, pp. 1193–1204.
- [14] E. Petrov, Analysis of sensitivity and robustness of forced response for nonlinear dynamic structures, *Mech. Syst. Signal Process.* 23 (1) (2009) 68–86.
- [15] M. Brake, C. Schwingshackl, P. Reuß, Observations of variability and repeatability in jointed structures, *Mech. Syst. Signal Process.* 129 (2019) 282–307.
- [16] A. Fantetti, L. Tamatam, M. Volvert, I. Lawal, L. Liu, L. Salles, M. Brake, C. Schwingshackl, D. Nowell, The impact of fretting wear on structural dynamics: Experiment and simulation, *Tribol. Int.* 138 (2019) 111–124.
- [17] C. Gastaldi, T.M. Berruti, M.M. Gola, The effect of surface finish on the proper functioning of underplatform dampers, *J. Vib. Acoust.* 142 (5).
- [18] M. Hüls, L. Panning-von Scheidt, J. Wallaschek, Influence of geometric design parameters onto vibratory response and high-cycle fatigue safety for turbine blades with friction damper, *J. Eng. Gas Turbines and Power* 141 (4).
- [19] A. Fantetti, C. Schwingshackl, Effect of friction on the structural dynamics of built-up structures: An experimental study, in: *Proceedings of ASME Turbo Expo 2020 Turbomachinery Technical Conference and Exposition*.
- [20] M. Lavella, D. Botto, M.M. Gola, Design of a high-precision, flat-on-flat fretting test apparatus with high temperature capability, *Wear* 302 (1–2) (2013) 1073–1081.
- [21] M.E. Kartal, D.M. Mulvihill, D. Nowell, D.A. Hills, Measurements of pressure and area dependent tangential contact stiffness between rough surfaces using digital image correlation, *Tribol. Int.* 44 (10) (2011) 1188–1198.
- [22] T. Hoffmann, L. Panning-von Scheidt, J. Wallaschek, Analysis of Contacts in Friction Damped Turbine Blades Using Dimensionless Numbers, *J. Eng. Gas Turbines Power* 141 (12).
- [23] A. R. Warmuth, P. H. Shipway, W. Sun, Fretting wear mapping: The influence of contact geometry and frequency on debris formation and ejection for a steel-on-steel pair, *Proc. R. Soc. A: Math., Phys. Eng. Sci.*
- [24] J. Hintikka, A. Lehtovaara, A. Mäntylä, Fretting-induced friction and wear in large flat-on-flat contact with quenched and tempered steel, *Tribol. Int.* 92 (2015) 191–202.
- [25] D. Infante-García, M. Marco, A. Zabala, F. Abbasi, E. Giner, I. Llavori, On the role of contact and system stiffness in the measurement of principal variables in fretting wear testing, *Sensors* 20.
- [26] D. Botto, M. Umer, A novel test rig to investigate under-platform damper dynamics, *Mech. Syst. Signal Process.* 100 (2018) 344–359.
- [27] L. Gallego, B. Fulleringer, S. Deyber, D. Nelias, Multiscale computation of fretting wear at the blade/disk interface, *Tribol. Int.* 43 (4) (2010) 708–718.
- [28] T. Butlin, G. Spelman, P. Ghaderi, W.J. Midgley, R. Umehara, Predicting response bounds for friction-damped gas turbine blades with uncertain friction coupling, *J. Sound Vib.* 440 (2019) 399–411.
- [29] T. Butlin, P. Ghaderi, G. Spelman, W.J. Midgley, R. Umehara, A novel method for predicting the response variability of friction-damped gas turbine blades, *J. Sound Vib.* 440 (2019) 372–398.
- [30] X. Delaune, E. de Langre, C. Phalippou, A Probabilistic Approach to the Dynamics of Wear Tests, *J. Tribol.* 122 (2000) 815–821.

- [31] T. Hoffmann, L. Panning-von Scheidt, J. Wallaschek, Measured and simulated forced response of a rotating turbine disk with asymmetric and cylindrical underplatform dampers, *J. Eng. Gas Turbines Power* 142 (5).
- [32] I.A. Sever, E.P. Petrov, D.J. Ewins, Experimental and numerical investigation of rotating bladed disk forced response using underplatform friction dampers, *J. Eng. Gas Turbines Power* 130 (2008) 4.
- [33] S. Ghosh, P. Pandita, S. Atkinson, W. Subber, Y. Zhang, N. C. Kumar, S. Chakrabarti, L. Wang, Advances in bayesian probabilistic modeling for industrial applications, *ASCE-ASME J Risk and Uncert in Engrg Sys Part B Mech Engrg* 6.
- [34] N. Metropolis, S. Ulam, The monte carlo method, *J. Am. Stat. Assoc.* 44 (247) (1949) 335–341.
- [35] J. Yuan, G. Allegri, F. Scarpa, R. Rajasekaran, S. Patsias, Probabilistic dynamics of mistuned bladed disc systems using subset simulation, *J. Sound Vib.* 350 (2015) 185–198.
- [36] M.D. McKay, R.J. Beckman, W.J. Conover, Comparison of three methods for selecting values of input variables in the analysis of output from a computer code, *Technometrics* 21 (2) (1979) 239–245.
- [37] J. Sacks, W.J. Welch, T.J. Mitchell, H.P. Wynn, Design and analysis of computer experiments, *Stat Sci.* (1989) 409–423.
- [38] C. Cortes, V. Vapnik, Support-vector networks, *Mach. Learn.* 20 (3) (1995) 273–297.
- [39] N. Wiener, The homogeneous chaos, *Am. J. Math.* 60 (4) (1938) 897–936.
- [40] D. Xiu, G.E. Karniadakis, The wiener–askey polynomial chaos for stochastic differential equations, *SIAM J. Sci. Comput.* 24 (2) (2002) 619–644.
- [41] E. Sarrouy, E. Pagnacco, E.S. de Cursi, A constant phase approach for the frequency response of stochastic linear oscillators, *Mech. Ind.* 17 (2) (2016) 206.
- [42] T. Roncen, J.J. Sinou, J.P. Lambelin, Non-linear vibrations of a beam with non-ideal boundary conditions and uncertainties - Modeling, numerical simulations and experiments, *Mech. Syst. Signal Process.* 110 (2018) 165–179.
- [43] A.M. Panunzio, L. Salles, C.W. Schwingshackl, Uncertainty propagation for nonlinear vibrations: A non-intrusive approach, *J. Sound Vib.* 389 (2017) 309–325.
- [44] J. Didier, J.-J. Sinou, B. Faverjon, Nonlinear vibrations of a mechanical system with non-regular nonlinearities and uncertainties, *Commun. Nonlinear Sci. Numer. Simul.* 18 (11) (2013) 3250–3270.
- [45] J.-J. Sinou, J. Didier, B. Faverjon, Stochastic non-linear response of a flexible rotor with local non-linearities, *Int. J. Non-Linear Mech.* 74 (2015) 92–99.
- [46] B. Sudret, Global sensitivity analysis using polynomial chaos expansions, *Reliab. Eng. Syst. Saf.* 93 (7) (2008) 964–979.
- [47] R. Rajasekharan, E. Petrov, Uncertainty and global sensitivity analysis of bladed disk statics with material anisotropy and root geometry variations, *Eng. Rep.* 1 (3) (2019) e12043.
- [48] T. Cameron, J. Griffin, An alternating frequency/time domain method for calculating the steady-state response of nonlinear dynamic systems.
- [49] E. Sarrouy, J.-J. Sinou, Non-linear periodic and quasi-periodic vibrations in mechanical systems—on the use of the harmonic balance methods, in: *Advances in Vibration Analysis Research*, InTech, 2011.
- [50] M. Krack, J. Gross, *Harmonic balance for nonlinear vibration problems*, Springer, 2019.
- [51] E. Petrov, D. Ewins, Analytical formulation of friction interface elements for analysis of nonlinear multi-harmonic vibrations of bladed disks, *J. Turbomachinery* 125 (2) (2003) 364–371.
- [52] A. Fantetti, C. Pennisi, D. Botto, S. Zucca, C. Schwingshackl, Comparison of contact parameters measured with two different friction rigs for nonlinear dynamic analysis, *International Conference on Noise and Vibration Engineering*.
- [53] S. Medina, D. Nowell, D. Dini, Analytical and numerical models for tangential stiffness of rough elastic contacts, *Tribol. Lett.* 49 (1) (2013) 103–115.
- [54] K. Pearson, Notes on regression and inheritance in the case of two parents, *Proc. R. Soc. London* 58 (1895) 240–242.
- [55] M. Baudin, A. Dufloy, B. Iooss, A.-L. Popelin, Open turns: An industrial software for uncertainty quantification in simulation, *arXiv preprint arXiv:1501.05242*.
- [56] N. Wiener, The homogeneous chaos, *Am. J. Math.* 60 (4) (1938) 897–936.
- [57] R.G. Ghanem, P.D. Spanos, *Stochastic finite elements: a spectral approach*, Courier Corporation (2003).
- [58] I.M. Sobol, Sensitivity estimates for nonlinear mathematical models, *Math. Modelling Comput. Exp.* 1 (4) (1993) 407–414.
- [59] T. Roncen, J.-J. Sinou, J. Lambelin, Non-linear vibrations of a beam with non-ideal boundary conditions and uncertainties—modeling, numerical simulations and experiments, *Mech. Syst. Signal Process.* 110 (2018) 165–179.
- [60] W. Xie, Y. Yang, S. Meng, T. Peng, J. Yuan, F. Scarpa, C. Xu, H. Jin, Probabilistic reliability analysis of carbon/carbon composite nozzle cones with uncertain parameters, *J. Spacecraft Rockets* 56 (6) (2019) 1765–1774.